Surface-Layer Wind Shear and Momentum Transport From Clear-Sky to Cloudy Weather Regimes Over Land

Koning, A. M.; Nuijens, L.; Bosveld, F. C.; Siebesma, A.P.; van Dorp, P. A.; Jonker, H. J.J.

DOI
10.1029/2021JD035087

Publication date
2021

Document Version
Final published version

Published in
Journal of Geophysical Research: Atmospheres

JGR Atmospheres

RESEARCH ARTICLE
10.1029/2021JD035087

Surface-Layer Wind Shear and Momentum Transport From Clear-Sky to Cloudy Weather Regimes Over Land

A. M. Koning[1], L. Nuijens[1], F. C. Bosveld[2], A. P. Siebesma[1,2], P. A. van Dorp[3], and H. J. J. Jonker[1,3]

[1]Delft University of Technology, Delft, The Netherlands, [2]Dutch Royal Meteorological Insitute (KNMI), De Bilt, The Netherlands, [3]Whiffle, Delft, The Netherlands

Key Points:

- Cloudy regimes have larger total momentum flux distributed over a deeper layer, with up to 30% of the surface flux present near the cloud base
- Clear-sky and shallow cumulus regimes have notably larger crosswind momentum fluxes in the boundary layer
- Convective cloud regimes have less surface layer wind shear than the clear-sky regime for a given surface layer

Correspondence to:
A. M. Koning,
A.M.Koning@tudelft.nl

Citation:
Koning, A. M., Nuijens, L., Bosveld, F. C., Siebesma, A. P., van Dorp, P. A., & Jonker, H. J. J. (2021). Surface-layer wind shear and momentum transport from clear-sky to cloudy weather regimes over land. *Journal of Geophysical Research: Atmospheres*, *126*, e2021JD035087. https://doi.org/10.1029/2021JD035087

Received 23 APR 2021
Accepted 5 OCT 2021

Abstract This study investigates how wind shear and momentum fluxes in the surface- and boundary layer vary across wind and cloud regimes. We use a 9-year-long data set from the Cabauw observatory complemented by (8.2×8.2 km^2) daily Large Eddy Simulation (LES) hindcasts. An automated algorithm classifies observed and simulated days into different cloud regimes: (a) clear-sky days, (b) days with shallow convective clouds rooted in the surface layer, with two ranges of cloud cover, and (c) non-convective cloud days. Categorized days in observations and LES do not always match, particularly the number of non-convective cloud days are underestimated in the LES, which likes to develop convection. However, the climatology and diurnal cycle of winds for each regime are very similar in LES and observations, strengthening our confidence in LES' skill to reproduce certain clouds for certain atmospheric states. Along-wind momentum flux profiles are similar across all regimes, but large cloud cover (convective and non-convective) days have larger total momentum flux distributed over a deeper layer, with up to 30% of the surface flux still present near cloud base. The clear-sky and especially shallow cumulus regime with low cloud cover have notably larger crosswind momentum fluxes in the boundary layer. Surface-layer wind shear at daytime is smallest in the shallow cumulus regimes, having deeper boundary layers and a steady increase in surface layer wind speed during daytime. Compared to clear-sky days at a similar stability, convective cloud regimes have smaller surface-layer wind shear and larger surface friction than estimated by Monin-Obukhov Similarity Theory.

Plain Language Summary Accurate modeling of surface wind speeds is required to improve wind energy prediction and representation of surface fluxes in models, as they influence a range of atmospheric processes. This paper compares the surface layer wind gradients and turbulent momentum fluxes among various wind and cloud regimes. We use observed and modeled climatological wind and cloud records over the Netherlands, which we grouped into (a) clear-sky days, (b) (cumulus) clouds that interact with the layer below, with two ranges of cloud cover, and (c) days not driven by convection. We have confidence in the modeled winds and clouds: when comparing the regime-averaged behavior of wind, temperature, and humidity; the model and observations show similar results. When comparing the different cloud regimes, we find more similar wind speeds at different altitudes on cumulus days. Shallow cumulus regimes appear to have larger surface friction than clear-sky regimes when correcting for atmospheric stability.

1. Introduction

Accurate predictions of wind speed and wind direction near the surface are important, for instance, to estimate energy generation in wind farms or to predict surface stress, heat, and moisture fluxes that influence a range of atmospheric processes. The short-term local wind forecast relies on many processes, of which several are not resolved in numerical weather prediction (NWP) models but parameterized. Unresolved parameterized processes that impact the winds are surface drag and shear-driven turbulence, as well as convection and gravity waves. Over land, the deepening of the boundary layer due to turbulence and dry convection is typically accompanied by the development of shallow cumulus clouds. The objective of this study is to investigate the relationship between wind shear and momentum fluxes with cloud or weather regimes and identify whether convective cloud regimes in particular, as opposed to clear sky regimes, have a different structure of wind and momentum flux near the surface.

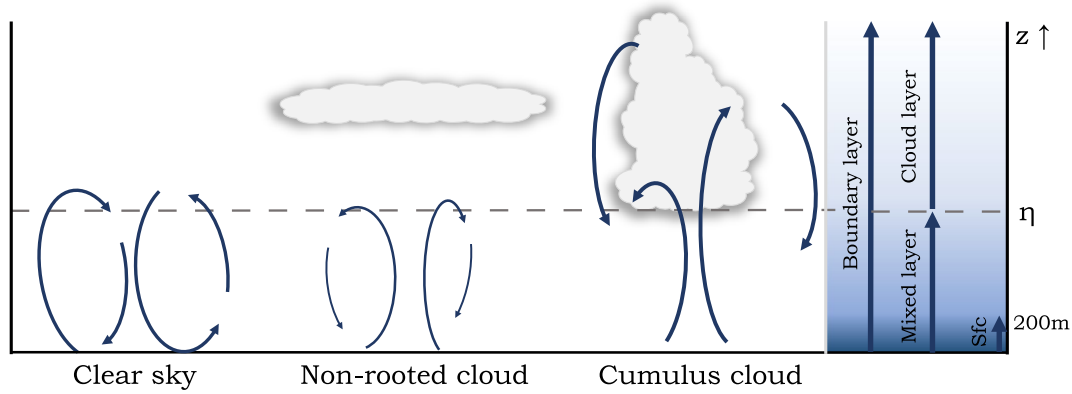

Figure 1. The main cloud regimes and associated boundary-layer scale circulations are shown. Stratus layers may obstruct a large part of the solar radiation, reducing the updraft strength. Thicker arrows correspond to stronger up- and downdrafts. The dashed horizontal line indicates the top of the mixed-layer (η). On the right, we specify the definitions of the boundary layer (for the cumulus regime), mixed-layer, cloud layer, and surface layer (indicated as "Sfc" and taken as the layer up to 200 m). In the cumulus cloud regime, the mixed-layer is identical to the sub-cloud layer, whereas in the clear-sky and non-rooted cloud regime the mixed-layer comprises the entire boundary layer.

There are a number of ways through which winds and clouds relate. First of all, clouds are inherently coupled to certain wind or weather regimes. For instance, in the Netherlands, cloudy days typically have westerly winds bringing moist air masses onto land, whereas days with easterly winds and high surface pressure tend to be associated with clear skies. Significant (deep) convective and stratiform cloudiness are associated with the passage of storm systems coming from the west, while congestus clouds prevail after cold-front passages and in cold air outbreaks from the north.

Second, as illustrated in Figure 1, clouds alter the surface energy budget through radiation, which influences turbulence and convection in the boundary layer. He et al. (2013) contrasted entirely cloud-free days (clear skies) over the Netherlands with days that have persistent low level cloudiness (cloud base height <1.5 km, at least 10 cloud base detections out of a maximum of 20 detections per 10 min) and found that winds in the surface layer are less well-mixed (have larger shear) on cloudy days, because of reduced incoming solar radiation at the surface and reduced surface buoyancy fluxes.

Third, shallow cumulus clouds are naturally rooted within the surface layer and develop as a result of thermal circulations driven by the surface buoyancy flux (that may already be larger on clear sky days). The turbulent mixing that drives clouds will also drive different winds. Detecting the convective plumes using the wavelet analysis, Schalkwijk et al. (2010) exposed the thermal structure in the boundary layer up to 200 m (in observations), as well as the full boundary layer (in Large Eddy Simulation [LES]). They found that thermals are responsible for 40% of the total vertical heat transport. Thermals can, however, also violate the often used Monin-Obukhov Similarity Theory (MOST) to estimate fluxes in the surface layer. Fodor et al. (2019) found that convective scale up and downdrafts may not have locally determined properties and may produce deviations from MOST estimated buoyancy flux in the limit of free convection. Even when MOST still holds, Li and Bou-Zeid (2011) found that momentum transport in the near surface layer (<10 m) became less efficient when the atmosphere became more unstable, opposed to buoyancy. They explained the lower efficiency by the increased importance of transport through convective plumes rather than through small-scale turbulent eddies.

Fourth, convective clouds may deepen the boundary layer and lead to deeper vertical mixing of scalars and wind (Stevens, 2007). Clouds may also alter turbulent circulations through mesoscale organization (Bretherton & Blossey, 2017; Holloway et al., 2017) or through evaporatively driven downdrafts, for instance, the gustiness associated with density currents driven by evaporation of rain (Jabouille et al., 1996, e.g.). Early flight campaigns showed that organization may change the turbulent momentum flux (LeMone & Pennell, 1976), measured in three convective situations over the ocean near Puerto Rico: on a suppressed day with almost no clouds, a day with shallow roll convection, and a day with enhanced shallow popcorn convection and numerous clouds. The two days with suppressed convective conditions had down-gradient

diffusive fluxes that act to reduce the wind shear, whereas the case with enhanced convection showed significant counter-gradient transport, especially below and near the bases of clouds, something that is typically associated with organized systems of deep convection (LeMone, 1983; LeMone & Jorgensen, 1991; Rotunno et al., 1988; Wu & Yanai, 1994; Tung & Yanai, 2002). Convective cloud organization is currently an important topic in the studies of trade-wind convection, where mesoscale variability in cloud, rain, wind, and scalars is pronounced (Bony et al., 2017).

Over land such studies are rarer (Moeng & Sullivan, 1994; van Stratum et al., 2014; Zhang & Klein, 2013), and the relationship between near-surface wind and convective or boundary layer tops is not well described. Much of what we know about momentum transport by shallow convection in fact stems from LES of cumulus convection over the ocean (ATEX, BOMEX, and RICO) (Brown, 1999; Saggiorato et al., 2020; Schlemmer et al., 2017; Zhu, 2015). Even for the ocean, such cases are highly idealized, with constant large-scale (wind) forcing and domains too small to allow for convective organization. Zhu (2015) exemplified just how different the simulated turbulent flux profiles are and can even change sign depending on cloud regime and the scales of the transport, for example, small-scale shear-driven eddies or larger coherent circulations. This motivates studying momentum flux profiles for a wider variety of cases and conditions as present in real nature.

In our study, we use a long climatology (2009–2016) of cloud and wind measurements collected at Cabauw (now part of the Ruisdael observatory [https://ruisdael-observatory.nl/]) to study how near-surface wind and momentum flux change with cloud regimes. Measurements by a ceilometer and a 200- m tall measurement tower are complemented by small-domain (8.2×8.2 km^2) LES runs of the same long period. The LES output provides insight into the turbulence processes, such as the momentum flux profiles, extending beyond 200 m. We distinguish non-convective days, clear-sky days, and days with clouds that are rooted in the surface layer (which we label convective clouds). Our analysis aims to answer how wind shear in the surface layer differs between these regimes, and whether convective cloud regimes are accompanied by different wind mixing behavior than the clear-sky regime, after accounting for differences in surface buoyancy fluxes, atmospheric stability, and large scale winds.

In the next section, we will describe the measurements taken at Cabauw, the set-up of the LES, and the selection method for the different cloud regimes. The cloud regimes as identified in the observations and in the LES will be verified and compared. In the results, we first describe the differences in wind mixing and momentum flux in the surface layer, using data from both observations and LES. Second, we will discuss differences for the entire boundary layer, for which only LES results are used. Conclusions are presented in Section 4.

2. Data

2.1. Cabauw (Ruisdael) Observational Data

The observational data contain 10-min interval measurements of wind speed and direction taken at the tower using cup anemometers and wind vanes. The anemometers and wind vanes are mounted on 10- m-long booms that are positioned at 40, 80, 140, and 200 m height. Because wind measurements are sensitive to flow obstructions, only the undisturbed measurements are selected from the three booms that measure wind direction and from two booms measuring wind speed. Winds at 10 and 20 m are measured at three different masts (70 and 140 m NE, 30 m SE from the main mast) to avoid flow disturbance by the main mast itself and the small buildings attached to the main mast. The selection of these separate masts depends on the wind direction. Momentum fluxes are estimated from wind measurements of sonic anemometers located at 3, 60, 100, and 180 m height, and are available every 10 min. They are corrected for streamline tilt due to flow obstruction around the masts and by instruments. Low frequency losses are corrected for according to Bosveld (1999). Further details can be found in Bosveld et al. (2020).

Cloud base height (cbh) is measured by an LD40 ceilometer. The LD40 is situated on a field to the south of the tower, within 50 m from the mast, which justifies synergistic use of the data (Bosveld, 2020). On this field, the net radiation and net surface fluxes are also measured. The ceilometer measures back-scatter intensity from particles using an 855- nm wavelength. The maximum range (detection height) is 13,600 m with a resolution of 7.5 m. It emits 65,000 pulses every 15 s, and returns three cloud base heights, as well as

vertical visibility and a precipitation index. We only use the first (lowest) measured cloud base, because the signal attenuates considerably after penetrating a cloud. Furthermore, we disregard any backscatter retrievals from altitudes above 5 km, as convective clouds have cloud bases below 5 km and we assume that clouds above 5 km do not have an influence on the mixed layer other than through radiation. The first detected cloud base height is not necessarily the height that corresponds to the lifting condensation level, where one expects convective clouds to have their base. It can correspond to cloud edges, sides of slanted clouds, or stratiform outflow. In Section 3, we describe in more detail how we use this information to classify cumulus days. Note that we make a clear distinction between cloud cover and cloud fraction. We refer to cloud cover as the areal fraction of the sky that is covered with cloud, which is measured by the ceilometer and can be calculated from the LES output. We use cloud fraction only to refer to the amount of cloud at any height; such profiles are only available from the LES.

2.2. Large Eddy Simulations

Our LES data are generated with the commercially used GPU-Resident Atmospheric Simulation Platform (GRASP), whose first version was based on the Dutch Atmospheric Large Eddy Simulation (DALES). For more information on DALES, we recommend reading (Heus et al., 2010). GRASP has been modified to run on Graphics Processing Units (GPUs) instead of Central Processing Units (CPUs), increasing the computational speed considerably, making it suitable for operational use in the wind energy industry. In our case, GRASP is run in hindcast mode, obtaining its daily initial and large-scale forcing conditions from European Centre for Medium-Range Weather Forecast's ERA5 data. This hourly forcing includes the radiative heating profiles, which means that the surface energy budget does not ”feel” the clouds resolved by LES, but those produced by the Integrated Forcasting System (IFS). Later we will see that this does not lead to a major difference as compared to the observations. For more information on the coupling to ERA5, please see Schalkwijk et al. (2015).

To enable the long period of daily hindcasts, the computations are limited to a domain of 8.192 by 8.192 km^2 by 5.079 km with a horizontal resolution of 64 m and a vertical resolution that decreases with height from 16 m near the surface to 80 m at approximately 5 km. This is notably smaller than what is currently common, but in line with benchmark LES studies (Siebesma et al., 2003; Stevens et al., 2001). Recently, Schemann et al. (2020) reflected on challenges in comparing point observations to large-domain LES, in which mesoscale flows evolve freely. They show that small domains remain closer to the synoptic conditions and therefore they are more suitable to compare with local observations.

The LES uses the sub-grid scheme of Sullivan et al. (1994). At the surface, MOST is applied in a local fashion, enabling a proper interaction between the surface and the overlying convective turbulence fields. Additionally, a heterogeneous surface model is applied to every gridbox individually, following TESSEL (IFS documentation cy41r1, 2015), using high resolution land use data from the CORINE (https://land.copernicus.eu/pan-european/corine-land-cover) data set. Apart from ensuring a correct local surface roughness, the heterogeneous surface conditions ensure a sensible roughness experienced by the in flowing wind. This roughness is similar to the average roughness in the domain due to periodic boundary conditions, which is reasonable as the region around the domain is quite similar to the conditions at Cabauw.

Each run is initialized at 21:00 UTC and runs to 23:59 UTC the next day. To avoid spin-up influences and overlap in the data, we use the output data from midnight to midnight. Data output consists of domain and hourly averaged profiles of wind, temperature, and humidity for the exact location of the Cabauw tower and liquid water path (LWP) snapshots are given every 10 min for the full horizontal scale of the domain, from which cloud cover is estimated.

3. Cloud Regime Classification

We identify three different cloud (weather) regimes:

1. Clear-sky regime (dry convective boundary layer).
2. Convective cloud (shallow cumulus regime).
3. Non-convective (other) cloud regime.

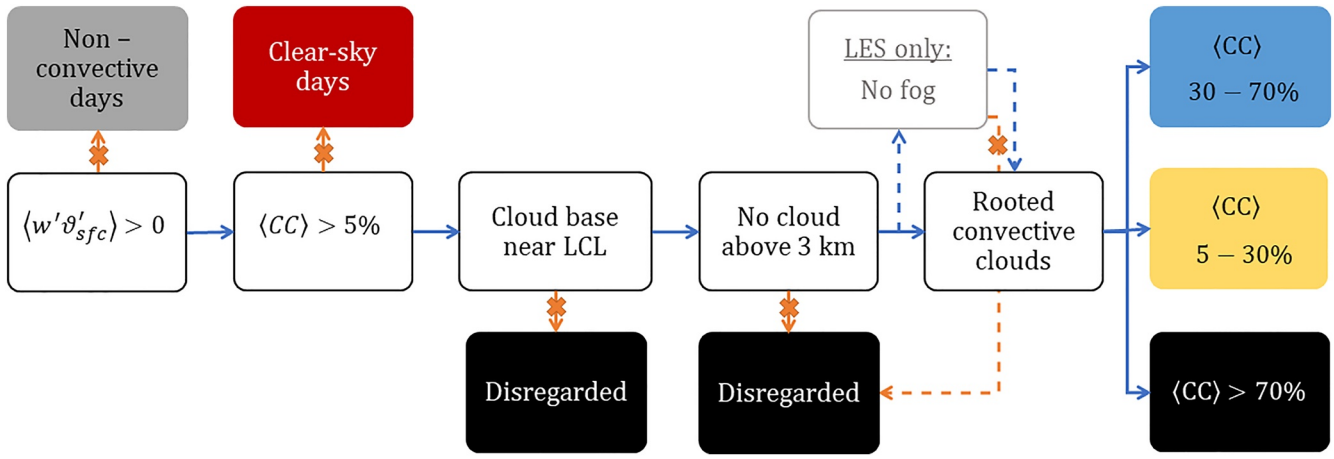

Figure 2. Process chart of the cloud regime classification. White boxes indicate the process steps, blue arrows indicate the criterion is met, and red arrows indicate that the criterion is failed. The colored boxes show the cloud regimes that are selected and the black boxes (including the convective cloud regime with cloud cover larger than 70%) indicate the disregarded days. Selection is between 10–16 UTC. Further explanation is found in the text.

The dry convective regime is assumed to represent convection in a boundary layer whose top lies below the lifting condensation level. The convective clouds are separated into two regimes: one with a cloud cover ranging between 5% and 30%, associated with very shallow convection (or forced clouds, such as cumulus humilis, to mediocris), the second with a cloud cover between 30% and 70%, which may be associated with larger clouds or cloud decks approaching stratocumulus. Convective days with more than 70% cloud cover consist of both stratocumulus clouds and deep convective clouds that often reach the top of the domain. Having its top at ~5 km, these clouds are likely not well-captured. Also, after the visual inspection, which is described next, we found that days with large cloud cover that are classified as convective clouds by the algorithm have a larger resemblance with stratus clouds that do not have a convective origin (both in observations and LES). This category is excluded in the remainder of the paper.

The visual classification has been executed for each day in 2016 to validate the automatic algorithm. For observations, we used the ceilometer backscatter to inform us about the growth of the boundary layer, whether cloud base grows with the boundary layer and whether there are multiple cloud layers. A hint of the presence of different cloud types can also be obtained. Satellite images (NASA's Moderate Resolution Imaging Spectroradiometer [MODIS] satellite images from Terra and Aqua, see https://worldview.earthdata.nasa.gov/), as well as the cloud camera provide further insight into the cloud type and the general cloud conditions around Cabauw. In the visual images and videos, we look at the cloud base, which should be flat for convective clouds, and at the structure: white tufts with cotton candy appearance and sharp cloud edges. Stratus clouds can be easily identified as a uniform gray cloud without sharp cloud edges, usually stretching out over a long distance. In LES, both cloud movies and the evolution of the cloud fraction profile are used for manual classification. For cumulus clouds, the cloud fraction usually peaks around the inversion height, becoming smaller toward the top. With cumulus congestus, another cloud fraction peak can be present higher up characteristic of stratiform outflow.

The procedure for automatic classification is shown in Figure 2. The white boxes indicate the process steps, the colored boxes show the cloud regimes that are selected, and the black boxes show days that were rejected from the data set. The brackets $\langle\cdot\rangle$ indicate averaging between 10 and 16 hr UTC (12–18 hr local summer time and 11–17 local winter time), for which the cloud regimes will be contrasted. This time interval includes the mean local solar noon at 11:40 UTC, as well as the cumulus clouds that form before noon and disappear around 12–15 hr UTC (season dependent). We first select all non-convective days with a negative average surface buoyancy flux. The clear-sky days are then obtained by taking days with an average cloud cover of less than 5% (allowing a small cloud to pass by). The amount of days that are in these cloud regimes are summarized in Table 1.

Days with convective clouds are then characterized by having cloud bases near the lifted condensation level. This poses two challenges: first, “what should we define as near LCL?”; and second, ”how do we handle

Table 1
The Total Number of Days are Shown Below for Both Observations and LES

	Obs	LES
Non-convective days	625	378
Convective days with clear-sky	316	482
Convective days with clouds	2,207	2,403
Total number of days	3,148	3,263

Note. The number of days that have been classified as non-convective, convective, and clear sky as well as the amount of convective cloudy days that will be next evaluated on having rooted clouds are shown. LES, Large Eddy Simulation.

days that have mostly convective clouds, but also (shorter) periods of non-convective clouds?" We introduce two parameters: the distance from the LCL (d) and fraction (f) of cloud bases within d from LCL between 10 and 16 UTC (observations) or fraction of time (LES) between 10 and 16 UTC with the lowest peak cloud fraction is near LCL. The settings for d and f are different for observations and LES, because they have other cloud measurements, which will be further discussed in the specific sections. Lastly, we added a restriction on the average amount of cloud at higher altitudes during daytime (< 5%), because the LES is not set up to produce deep convection.

3.1. Cloud Bases, Cloud Cover, and LCL in Observations

In observations, cloud-related properties such as cloud cover and cloud fraction above a certain height are inferred from the cloud base height measurements that are provided by the LD40 every 15 s if any cloud base is present. Temporal cloud cover is constructed by dividing the number of detected cloud bases in 10 min by the total number of measurements (40 in total). LCL is obtained by converting Bolton's formula for temperature at LCL (Bolton, 1980) to a height from each temperature, relative humidity, and specific humidity measurement at the tower at 200 m altitude during 10:00–16:00 UTC (Romps, 2017). The settings for d and f are evaluated using visual inspection. If more than 1/3 of the detected cloud bases are near LCL, this day is flagged as a day with convective clouds. The 1/3 is subjectively chosen and evaluated, using visual inspection.

Comparing again with the manual classification and judging from the ceilometer quicklooks, we removed all days with more than 5% of its measured cloud bases above 3 km, to ensure the shallow convective regimes predominantly include shallow clouds. The sensitivity to the different thresholds are presented in Table 2.

3.2. Cloud Bases, Cloud Cover, and LCL in LES

In LES, 10-min averaged aerial cloud cover is calculated from the vertically integrated LWP. The cloud base height is taken as the first height at which the hourly and domain-averaged cloud fraction profile maximizes. To avoid detecting small excursions from zero as the local cloud fraction maximum, we set a minimum value of 1% cloud fraction. If no maximum exists (e.g., when the upper domain is saturated with cloud), we use the first height at which the cloud fraction exceeds 1%.

The main difference between the selection method in observations and LES is the criterion to check whether clouds are rooted. LES gives a cloud fraction averaged over the hour, whereas in observations we have data every 15 s. Therefore, the hourly cloud fraction in LES is likely to have clouds every hour, leading us to look only at whether (some) cloud is present during the individual hours. The sensitivity to the thresholds of the distance to LCL and the fraction of hours at which cloud base is near LCL is presented in Table 3.

Table 2
Number of Days in Each of the Two Convective Cloud Regimes in Observations for Different Settings of the Distance From Cloud Base to LCL (D) and the Fraction of the Amount of Measured Cloud Bases Between 10 and 16 UTC That Must Satisfy This Condition

Observations	CC 5%–30%	CC 30%–70%
d = 100 m, f = 33%	143	167
d = 150 m, f = 33%	165	253
d = 200 m, f = 33%	171	136
d = 200 m, f = 50%	157	189
d = 200 m, f = 70%	122	96

Note. Cloud cover above 3 km does not exceed 5%.

The LES is not sensitive to changing the allowed distance to LCL from 150 to 200 m, unlike observations, but it is sensitive to changing d from 100 to 150 m. Comparing again with the visually assessed days, we find that f = 4/7 and a limitation on cloud fraction above 3 km yield the best classification. For simplicity, we kept d to 200 m, as in the observations.

3.3. Validating the LES Against Observations

Intuitively, we expect more non-convective days in winter and more clear-sky or fair-weather cumulus days in the spring and summer months. This is reflected in the distribution of the cloud regimes over the different months, whose character is similar in observation and LES (Figure 3). The distribution of days falling into each cloud regime shows low cloud cover cumulus days become more numerous from spring to summer and

Table 3
Number of Days in Each of the Two Convective Cloud Regimes in LES for Different Settings of the Distance From Cloud Base to LCL (D) and the Fraction Hours Between 10 and 16 UTC That Must Satisfy This Condition

LES	CC 5%–30%	CC 30%–70%
$d = 100$ m, $f = 4/7$	190	416
$d = 150$ m, $f = 4/7$	231	449
$d = 200$ m, $f = 4/7$	238	453
$d = 200$ m, $f = 3/7$	273	462
$d = 200$ m, $f = 5/7$	191	438

Note. Average cloud fraction above 3 km does not exceed 5%. LES, Large Eddy Simulation.

decline again in autumn. The confusion matrix, which compares days classified in LES and observations for the entire climatology, reveals an overall good agreement in the relative distribution of days into different cloud regimes (Table 4). We can see in the cumulus regimes that LES often produces too little or too much cloudiness, and the LES appears to favor the formation of convective clouds compared to the observations: more convective days are categorized from the LES at the expense of non-convective (cloud) regimes. We believe that the limited domain and a lack of variance in the large-scale forcing both play a role in constraining the LES' skill in reproducing cloud systems much larger and deeper than the domain size used and that the cyclic boundary conditions and a lack of cloud radiative feedbacks may overemphasize convective structures. Coupling LES to large-scale flows in realistic ways remains an area of active research, whereby moving to large domains does not necessarily imply better comparisons with local observations (Schemann et al., 2020).

In the remainder of our study, we compare statistics within the cloud regimes, which as these tables indicate, do not necessarily include the exact same days. This is not a concern, because our objective is not to check whether the LES captures daily weather, but instead we are looking to expose the physics that accompany specific cloud regimes. As we will show next, the observations and the LES largely agree on the weather conditions that accompany the different cloud regimes.

4. Climatology of Cloud Regimes

Figure 4 shows histograms of observed mean temperature, relative humidity (RH), zonal and meridional wind speed (averaged over the lowest 200 m), and surface buoyancy flux during the daytime hours (10:00–16:00 UTC) for the four cloud regimes. Typical continental fair weather in the convective regimes is associated with warm and relatively dry surface layers and positive buoyancy fluxes (by definition). This reflects that such regimes are most common in spring and (early) summer (Figure 3). The cloudier regimes occur on days with larger RH, which in the case of the non-convective regime is frequently in winter and likely associated with storm passages and (by definition) negative surface buoyancy fluxes. Cloudy days are generally days with westerly winds, which bring relatively moist air from the ocean on to land, whereas a relatively large portion of the clear sky days happen when winds are from the east. Convective clouds are not restricted to warm fair-weather. The Netherlands experiences regular occurrences of cumulus congestus and even deeper convection on days with cold air outbreaks (typically northwesterly winds) and after frontal passages (typically southwesterly winds). Some of which might be present in the CC 30%–70% regime, although we believe most are filtered out in our cloud classification.

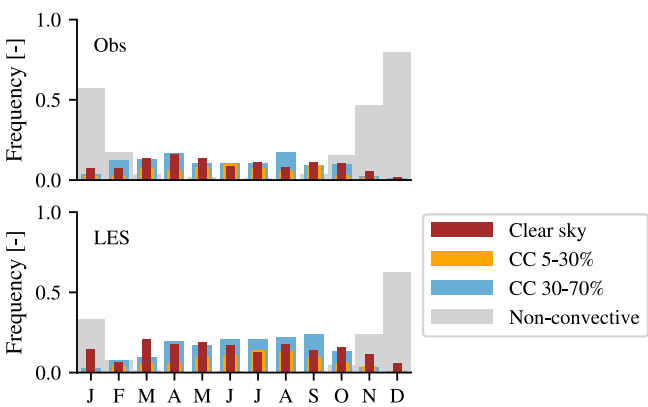

Figure 3. Distribution of the cloud regimes per month for years 2009–2017. Upper panel: Observations, lower panel: Large Eddy Simulation.

Figure 5 shows a similar climatology for the LES, but then in terms of averaged vertical profiles of cloud fraction, thermodynamics and the horizontal wind components extending up to heights of approximately 5 km. To maintain vertical structure, the height axis is scaled by the mixed-layer height (η), defined as the height of the minimum buoyancy flux and often coinciding with cloud base. The cloud fraction profiles confirm our classification, revealing the classical cumulus cloud fraction profile for the cumulus regimes (yellow and blue lines). The non-convective regime (e.g., westerly storms, in gray) also contains days with fog and other stratus layers. Like the histograms (Figure 4), the clear sky and cumulus days are warm and relatively dry, with weaker westerlies or even easterly winds. Profiles of virtual temperature are well mixed in all cloud regimes. The mixed-layer height is clearly visible

Table 4
Confusion Matrix Comparing the Cloud Regime Selection in Observations and LES

		LES					
		Clear sky	CC 5%–30%	CC 30%–70%	CC > 70%	Non-convective	Total obs
Observations	Clear sky	243	26	8	3	0	280
	CC 5%–30%	18	80	47	2	0	147
	CC 30%–70%	7	44	139	35	0	225
	CC >70%	0	2	39	125	16	182
	Non-convective	33	5	19	29	352	438
	Total LES	301	157	252	194	368	1,256

Note. LES, Large Eddy Simulation.

in the temperature, relative humidity as well as the wind speed profiles and often coincides with cloud base height.

From a careful observation of the wind profiles, we can already notice that the zonal u wind is well mixed in the boundary layer in all regimes, except the non-convective regime. In turn, these have a larger wind turning throughout the boundary layer, reflected by larger wind shear (vertical gradients) in the meridional component. In the following, we will look more closely at wind shear in the surface layer and address whether there are notable differences in how winds are vertically mixed depending on the regime.

5. Wind Gradients in the Surface Layer

To address surface layer wind gradients and the degree of wind mixing in the morning and afternoon, we adopt the analysis of He et al. (2013) and plot wind speeds at different heights as a diurnal cycle. We do this for both the observations and the LES (Figure 6). Because the observation heights are not the same as the LES grid heights, we interpolated the LES wind linearly to the observation heights. The general characteristic of the wind diurnal cycle is a larger wind gradient (wind shear) during the night and a smaller wind shear during the day. During the night, the boundary layer becomes shallower and stratified, and turbulent mixing is reduced. At Cabauw, the boundary layer height sometimes becomes smaller than the tower enabling us to detect nocturnal low level jets (LLJ). LLJs are measured 20% of the nights, usually between 140

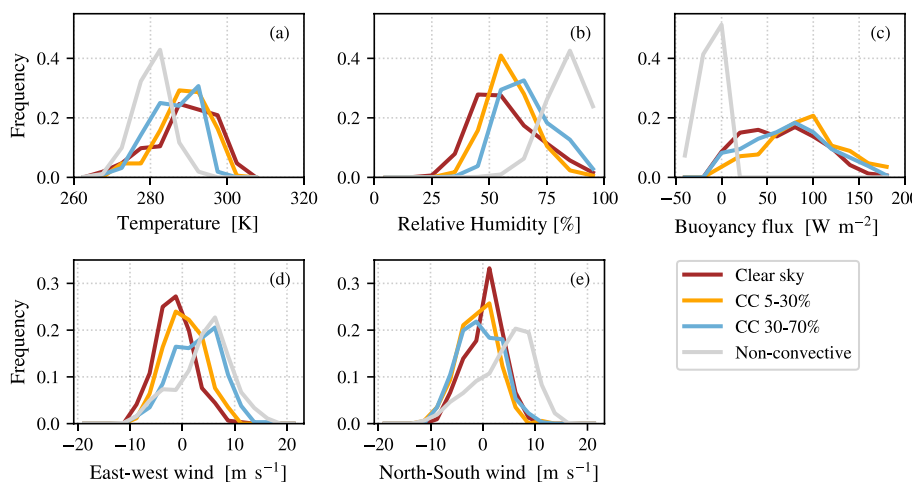

Figure 4. Distribution (histogram) of observed temperature, relative humidity, surface buoyancy flux, zonal wind u, and meridional wind v for each cloud regime. Positive zonal winds indicate winds from the west and positive meridional winds indicate winds from the south. Except for the surface buoyancy flux, all variables are averaged over the lowest 200 m and between 10 and 16 hr UTC.

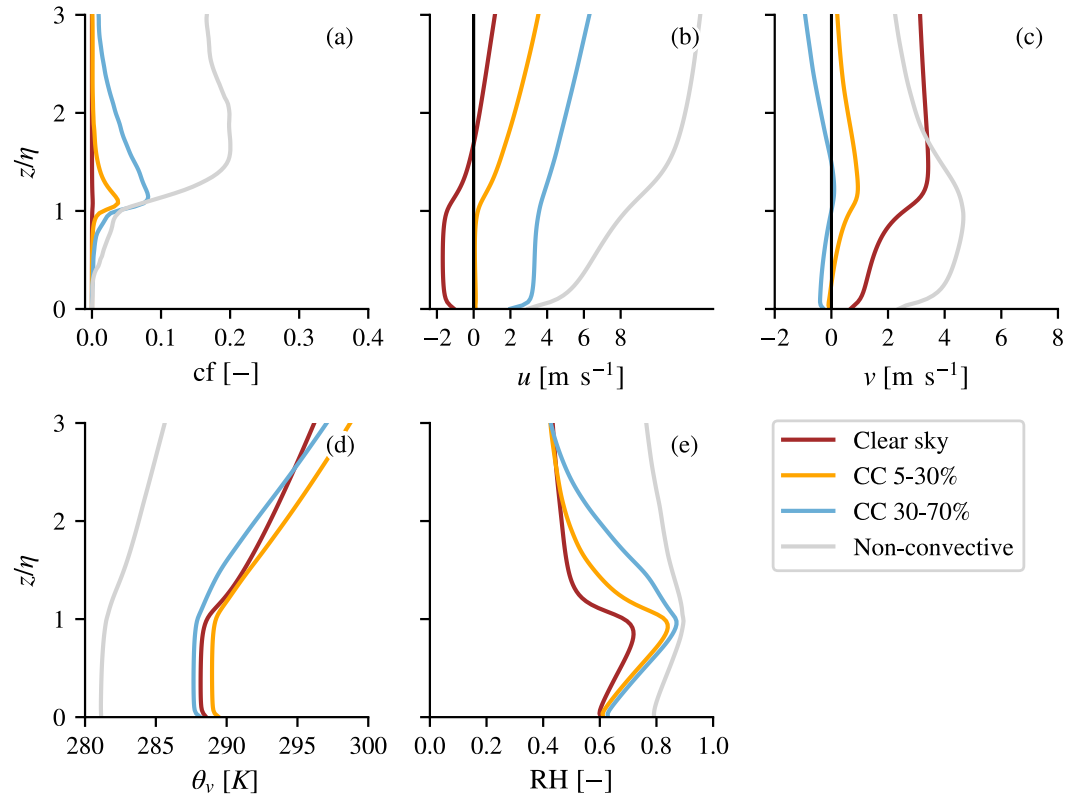

Figure 5. Large Eddy Simulation cloud regime averaged profiles of (a) the cloud fraction, (b) zonal wind speed (positive eastward) u, (c) meridional wind speed (positive northward) v, (d) θ_v, and (e) relative humidity.

and 260 m above the surface and with wind speeds from 6 to 10 m s^{-1} (Baas et al., 2009). The development of the wind during the day is in each regime well-captured by LES (Figure 6). The main difference with the observations is in the wind speed. At night, the LES has faster winds between 80 and 200 m, whereas during the daytime, observations usually show a stronger mean wind at 10 m. The wind bias at nighttime is a known issue in IFS, and a weak bias is also found in ERA5 through which the LES may inherit this wind bias. This should not affect the ability of the LES to reproduce the turbulence that underlines the convective influences we are studying here.

During daytime, wind shear is reduced in all regimes, especially between 80 and 200 m. The smallest wind shear (strongest mixing) is observed on shallow convective days, followed by clear-sky days. Based on the study by He et al. (2013), we expect better mixing on days with larger surface buoyancy flux, which is the case. The cumulus and clear-sky days have the largest surface buoyancy fluxes (Figure 4c). The more cloudy non-convective regime, with negative surface buoyancy fluxes, has larger vertical shear and mixing is almost absent.

At all height levels, wind speed in the surface layer increases during daytime in the clear-sky and cumulus regimes. This may be caused by the deepening of the boundary layer, leading to the entrainment of higher momentum air from the free atmosphere into the boundary layer. Indeed, the cumulus regimes are associated with deeper mixed layers, whose tops are identified as the minimum of the surface buoyancy flux (Figure 7). Increases in wind speeds may also be connected to sea breeze effects, which have been observed in ~8.3% of the days from May to August (Arrillaga et al., 2018).

Figures 8a and 8b show that the total momentum flux ($\tau = \left(\overline{u'w'}^2 + \overline{v'w'}^2\right)^{1/2}$) at 60 m increases during daytime and peaks slightly after noon when the buoyancy flux is large (panel c and d). At 12:00 UTC, when the wind shear is smallest in the cumulus regimes, the total momentum flux is slightly larger in the shallow convective regimes than in the clear-sky regime. Likely because these regimes have larger near-surface wind

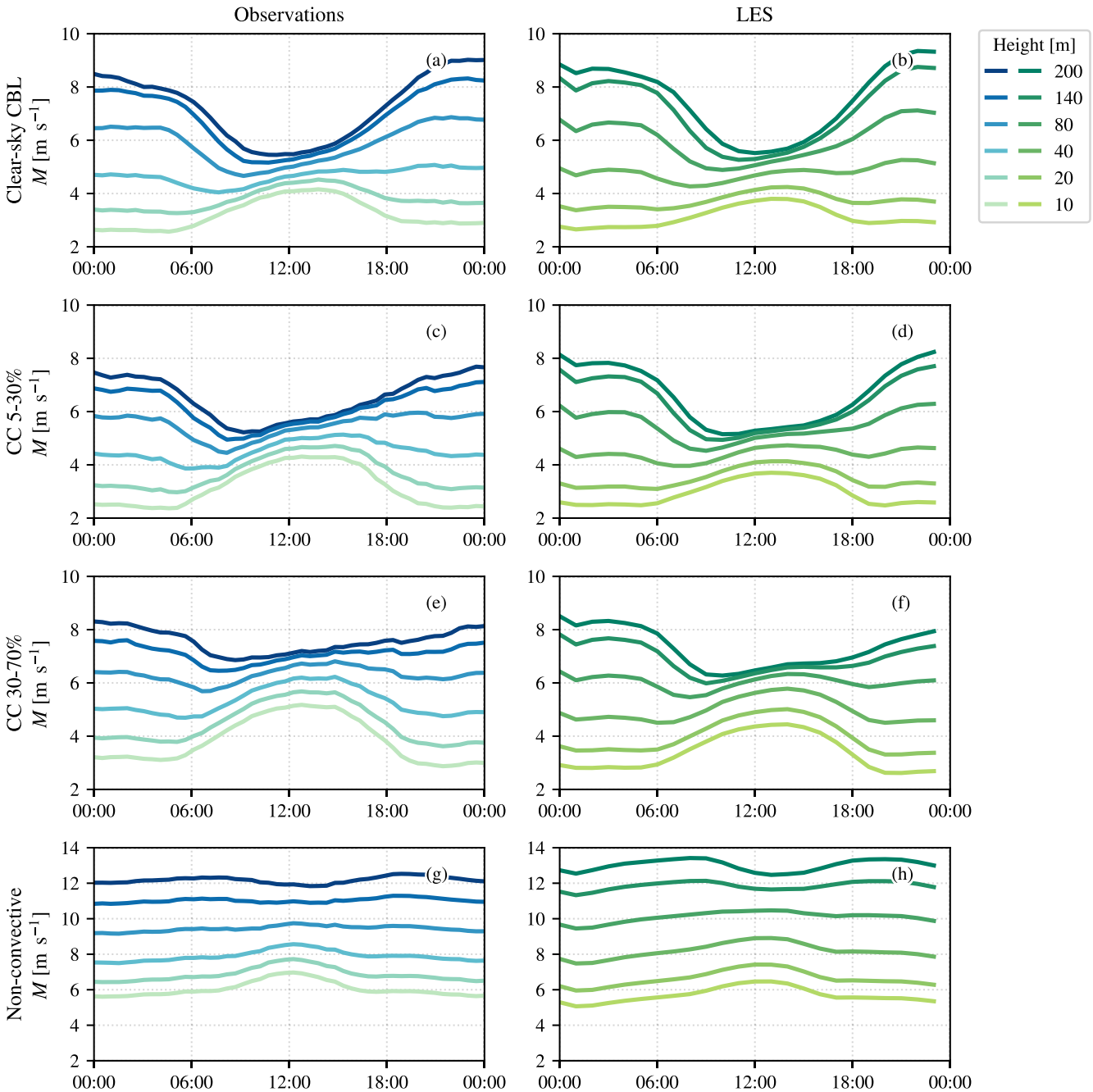

Figure 6. Average diurnal variations of wind speed (M) at five levels of the measurement tower at Cabauw under different cloud regimes. Observations (left column) and Large Eddy Simulation (right column) between 2009 and 2017 (incl.) are shown.

speeds at daytime (Figure 6). The 3 m momentum flux observations are different than the measurements at 60, 100, and 180 m. Because of the much smaller footprint at 3 m, it only experiences roughness from the low-grass meadows in Cabauw, whereas the measurements at higher altitude are influenced by rougher surfaces further away. Therefore, we chose to show the more representative 60 m measurements.

The total momentum flux in the non-convective cloud regime differs substantially between LES and observations, which cannot be explained by wind speed differences (they are comparable) and for now are not yet understood.

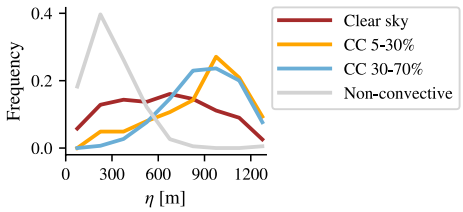

Figure 7. Distribution of the mixed layer top (η) within each cloud regime between 10 and 16 hr UTC from Large Eddy Simulation.

Evidently, the different climatology (weather regimes) associated with the different cloud regimes plays an important role in the degree of wind mixing in the surface layer. For example, fair weather cumulus days form on days with larger buoyancy fluxes, weaker stability, and weaker large-scale winds. Therefore, wind shear is by definition already smaller. In the following section, we account for the differences in stability and large-scale wind to identify which differences in wind shear across cloud regime remain.

5.1. Nondimensional Wind Gradients Following Monin-Obukhov Similarity Theory

Differences in wind speed and buoyancy flux are observed between clear-sky and shallow convective days. Stronger winds and weak buoyancy flux may introduce a very different mixing structure and momentum transport than on days with weaker winds and stronger buoyancy flux (Moeng & Sullivan, 1994). The effect of the surface buoyancy flux and the large-scale wind is illustrated in Figure 9. The wind speed at the surface must go to zero, and therefore, the wind shear is largely determined by the 200 m wind. In Figure 9, we normalize the wind by the daily average wind

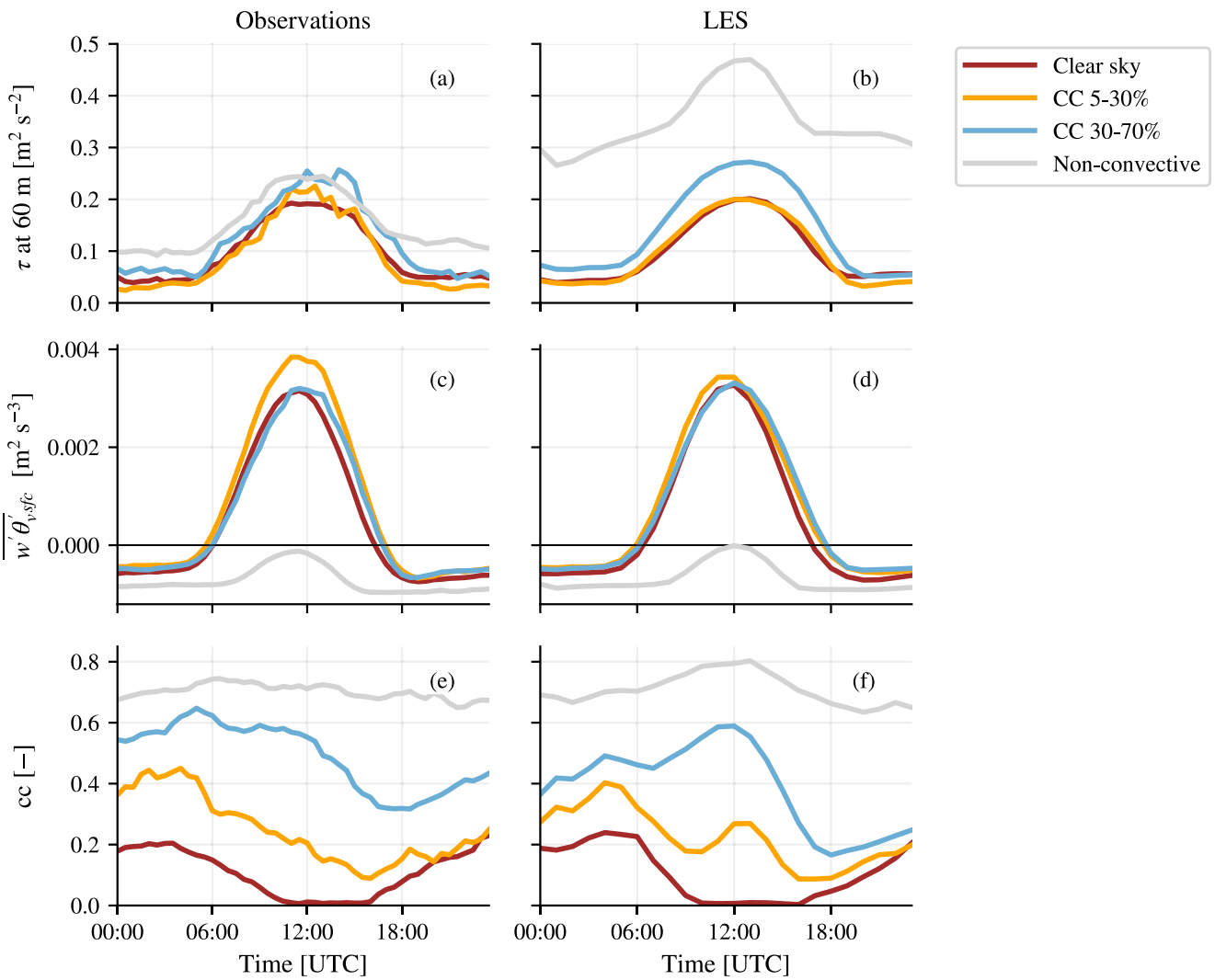

Figure 8. Average diurnal cycle of the total momentum flux (τ) at 60 m for each cloud regime in (a) observations and (b) Large Eddy Simulation.

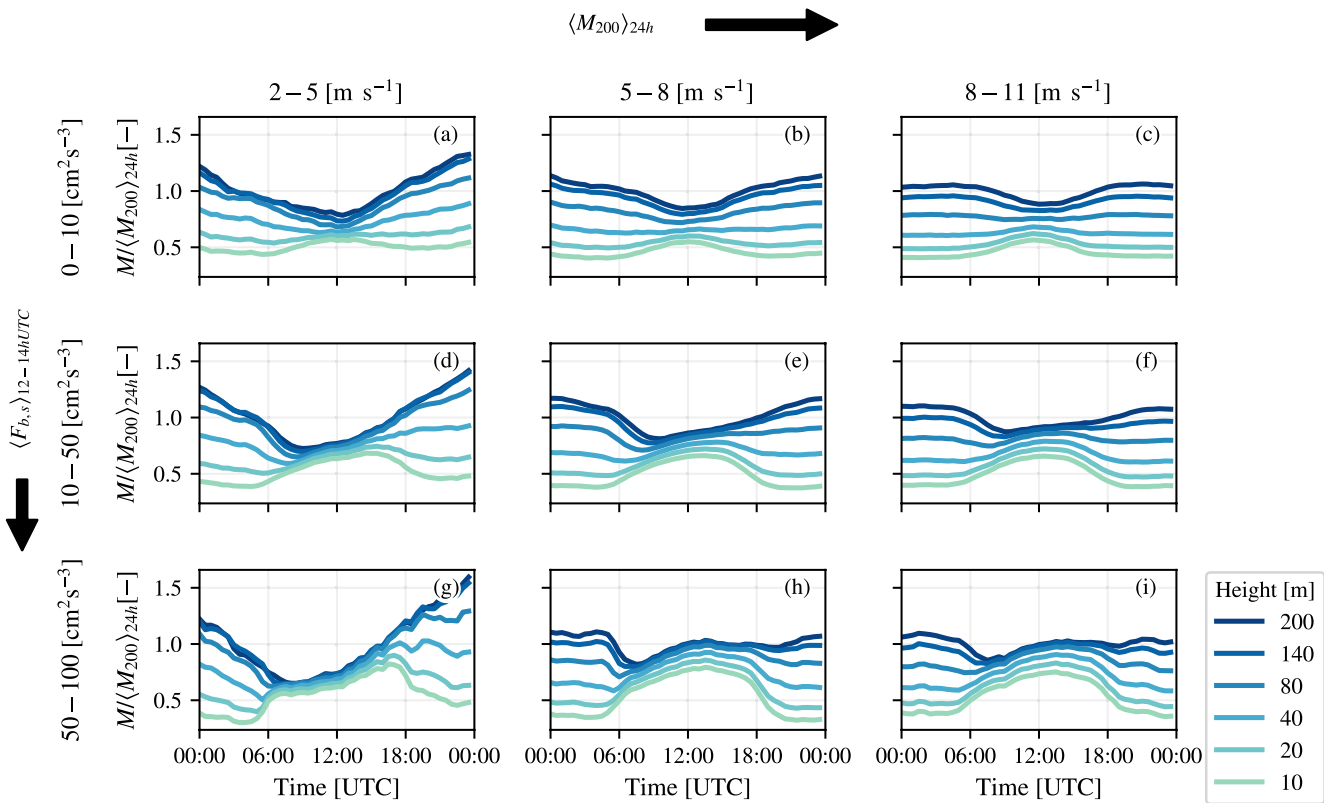

Figure 9. Diurnal cycle of wind speed as observed at the Cabauw tower when the data are separated on 12–14 hr UTC average surface buoyancy flux and daily average wind speed at 200 m.

speed at 200 m and show the composite diurnal cycle for days in three different surface buoyancy flux categories (on the *y*-axis) and three different 200 m wind categories, where we take the 200 m wind as a measure of the strength of the large-scale wind. The stronger the wind (toward the right in each row), the larger the shear. An increase in the surface buoyancy flux also leads to better mixed winds at first, but increasing it beyond 50 cm^{2}s^{-3} does not make a major difference, other than making the winds more variable and causing a stronger increase in wind speed during the afternoon.

To account for the covariability between wind and stability with convection, we use the Obukhov length. The Obukhov length (L), given by:

$$L = -\frac{\overline{\theta_v}}{kg}\frac{u_*^3}{(\overline{w'\theta_v'})_s}, \tag{1}$$

in which θ_v stands for the virtual potential temperature near the surface, u_* for the friction velocity at the surface, k for the von Kármán constant, g for the gravitational acceleration, and $(\overline{w'\theta_v'})_s$ for the surface buoyancy flux. The friction velocity u_*, defined as $u_* = (\overline{u'w'_{sfc}}^2 + \overline{v'w'_{sfc}}^2)^{1/4}$, denotes the turbulent momentum flux at the surface and is thus a measure of momentum destruction in the surface layer. Convective and stable conditions are distinguished by the sign of the buoyancy flux: a negative Obukhov length corresponds to a positive surface buoyancy flux and a more unstable atmosphere. Furthermore, a large negative Obukhov length implies either a small buoyancy flux and/or a large friction velocity, and thus more neutral conditions, whereas a small negative Obukhov length indicates more unstable conditions.

If we contrast the different cloud regimes *at a given Obukhov length*, we may identify whether processes other than stability play a role in setting the surface layer wind shear. Figure 10 shows two parameters as function of classes of stability ($-1/L$), which are all averaged between 12:00 and 14:00 UTC, where wind speeds in the diurnal cycle were best mixed. We only look at an unstable atmosphere ($-1/L > 0$, with weak-

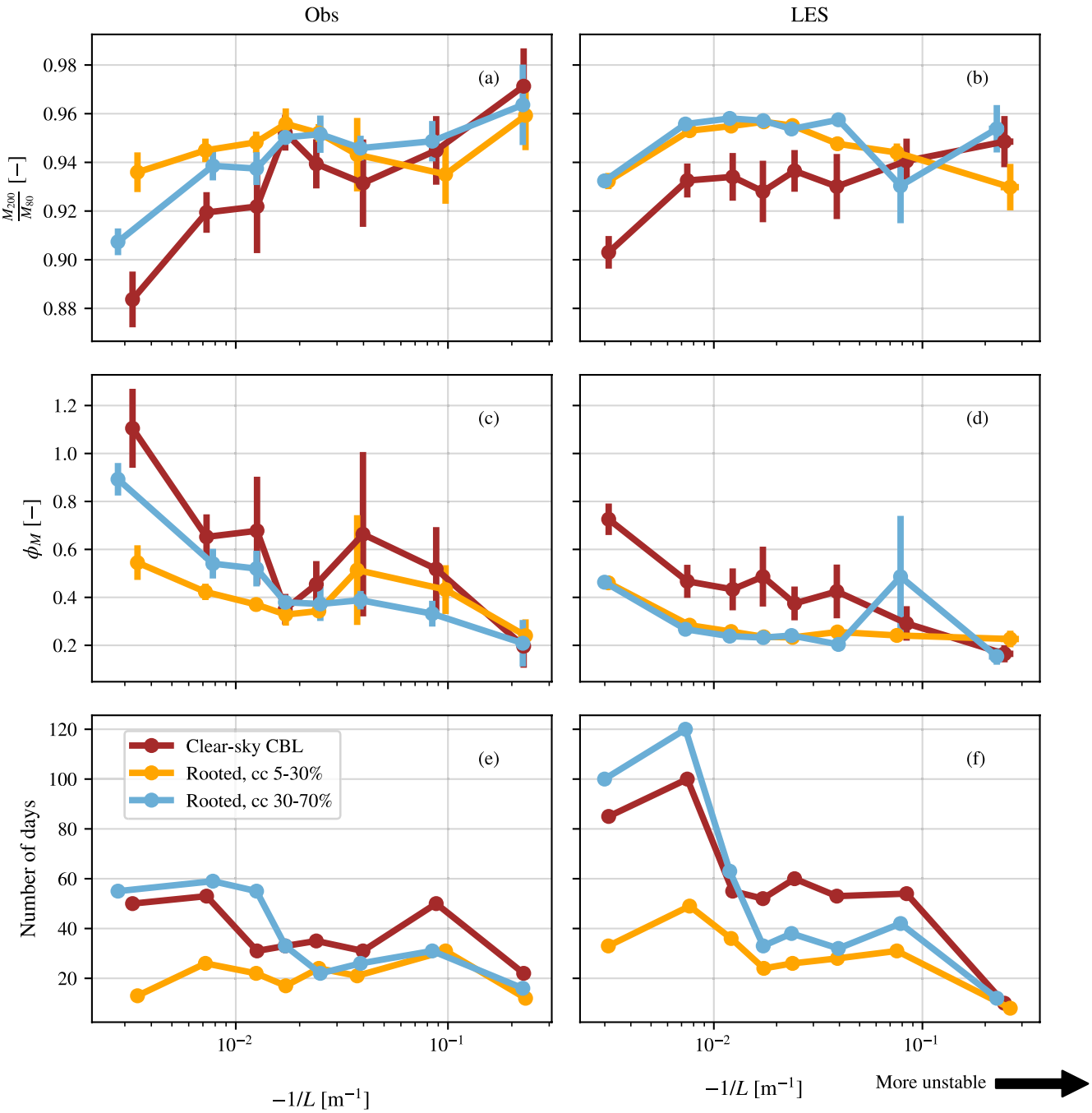

Figure 10. Observations (left) and Large Eddy Simulation (right): (a, b) Ratio between the wind speed at 80 and 200 m, (c, d) universal similarity functions, and (d, e) the number of days within each −1/L bin for the five cloudiness categories. Error bars in panel (a–d) indicate the standard error of the mean. All data are averaged over the hours 12–14 UTC, when the winds are best mixed.

ly unstable (more neutral) conditions on the left and more unstable conditions on the right). Panel a and b show the ratio of the 80 and 200 m wind, as a measure of the wind shear: the closer the ratio to 1, the smaller the shear. Panels c and d show the universal similarity function ϕ_M(z/L), commonly known from the Monin-Obukhov Similarity Theory (MOST), which is defined as:

$$\phi_M = \frac{\kappa z}{u_*}\frac{\partial u}{\partial z}. \quad (2)$$

We approximate ϕ_M from the 12:00 to 14:00 UTC averaged winds and estimate $\partial_z u$ from M_{80} and M_{200}. ϕ_M is another way of looking at wind mixing, but it also allows to remove a hidden dependency on u_*. The general behavior of ϕ_M is to decrease from neutral to unstable conditions as L is reduced (toward the right).

In the observations (left panels), across all stability classes, the regimes with convective clouds with cloud covers 5%–30% and 30%–70% (yellow and light blue) have a relatively larger M_{80} to M_{200} ratio than the clear-sky regime (red). This also shows in the ϕ_M curves. The regimes have separate curves, whereby the convective cloud regimes (yellow and light blue) exhibit smaller ϕ_M values than clear skies. In other words, at a given wind gradient these regimes have larger frictional velocity (larger momentum fluxes) near the surface. This suggests that deeper or stronger convective circulations sustain larger 80 m wind speeds compared to a situation where only shear-driven turbulent stresses are present. The vertical bars indicate the standard error and reveal that variability is larger in more unstable classes. These classes also include less samples (days), but it may also reflect that convective scales do not make a large difference when the atmosphere is already unstable.

The LES (right panels) confirms this picture, although there are notable differences. For instance, values for ϕ_M are overall smaller in LES than for the observations, which is probably because the observed and simulated roughness lengths are different. Cabauw is known to have a complicated land surface, with grassland and small roughness lengths felt close to the surface and trees and a larger roughness length felt at greater heights.

In general, the LES reproduces the different character of the momentum mixing under clear skies and (shallow) convective days, and therefore, we can examine additional statistics from the LES. As we saw earlier in Figure 7, the convective cloud regimes are associated with deeper mixed layers. Next, we will explore wind profiles and momentum flux profiles for the different regimes across the entire boundary layer and not just near the surface.

6. Wind and Momentum Flux Profiles in the Boundary Layer

Can we identify differences in momentum transport between cloud regimes? This is where the LES output is particularly valuable, because it provides momentum fluxes at height levels extending beyond the tower height. Not only the wind speed, but also the wind direction varies at Cabauw. For instance, there are regular episodes with easterly winds and westerly winds in the clear sky regime, see Figure 4. Changes in wind directions are associated with a change in sign of the momentum flux, which upon averaging, can bias the momentum flux toward small or zero values. We therefore transform the winds to a natural coordinate system whereby the positive (streamwise) s axis at every height level points in the direction of the hourly mean of the wind at 60 m height, while the (normal) n axis is defined perpendicular and anti-clockwise from the positive s axis. The along-wind and cross-wind momentum fluxes are calculated for each height and are then normalised by the friction velocity squared and plotted against the nondimensional height axis z / η. The mean along-wind and crosswind profiles for each regime are shown in Figures 11a and 11b. In essence, the crosswind component tells us how the wind is turning with height in the boundary layer with the wind at the lowest 10% of the mixed layer as a reference. A negative crosswind implies a (clockwise) veering of the wind with height. The average flux corresponding to a veering or backing crosswind is similar of shape but has a different sign (panel e). In the cumulus regimes, the magnitude of the flux differs between backing and veering winds: the slower backing winds have smaller (normalised) fluxes for the low cloud cover convective regime, whereas for the higher cloud cover convective regime the behavior is reversed. The general tendency is similar for all cases: in the lower mixed-layer the wind is slowed down, whereas in the upper part the crosswind is typically sped up. As in Figures 5d and 5e, days that are not convectively driven tend to have strong westerly winds (e.g., storm passages) and larger wind shear across the mixed-layer. The crosswind component for z / η < 1 is small in all regimes, implying a well-mixed sub-cloud layer. Substantial wind turning is pronounced near the mixed-layer height (or cloud base).

The other panels in Figure 11 show the skewness of the vertical velocity (c) and the nondimensional along- and crosswind fluxes (d, e), as well as the total momentum flux τ (f). Note that the average of the total momentum flux τ is unequal to the sum of the average along- and crosswind fluxes as we first calculate τ, normalize it, and then average over each cloud regime. The momentum fluxes clearly reveal how turbulent

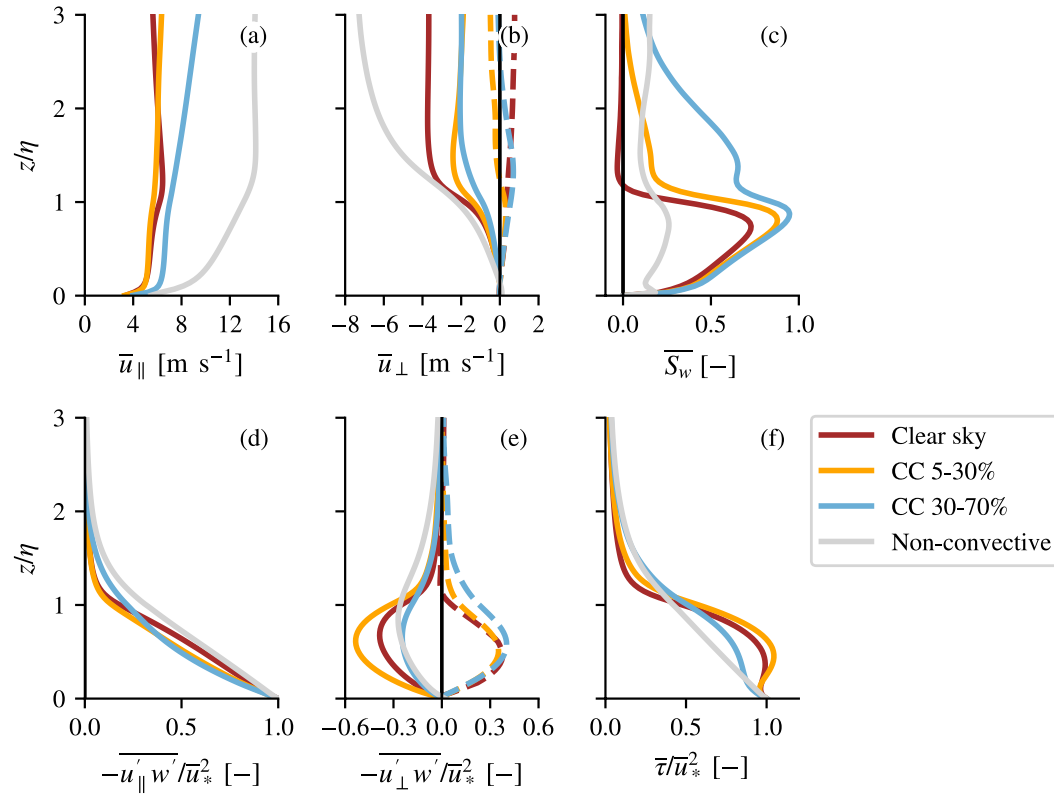

Figure 11. Cloud regime averaged Large Eddy Simulation profiles of the (a) mean wind, (b) cross wind, (c) skewness of vertical wind, momentum fluxes in (d) parallel and (e) crosswind direction, and (f) total flux for the five cloud regimes. Dashed lines in panels (b) and (e) indicate the backing wind cases. All variables are normalized by the mixed-layer height, fluxes are also normalized using the surface friction velocity.

mixing extends beyond $z/\eta = 1$ for the cloudier categories (light blue to gray). For instance, the normalized total momentum flux τ decreases with height approximately linear (Figure 11f), but is still at least 30% that of its surface value at $z/\eta = 1$ for the often overcast non-convective regime in gray, as well as the high CC cumulus regime in light blue.

The clear-sky and cumulus regimes have a normalized total momentum flux at $z/\eta = 0.5$ that is close to 1 (Figure 11f). The relatively large flux is primarily generated in the crosswind component (Figure 11e). The strong wind turning or wind jump at the top of the mixed layer can play a role at producing larger shear-driven stresses. Additionally, (convective) eddies can contribute to flux at these levels. These regimes (in blue and yellow) have the largest vertical velocity skewness in the sub-cloud layer (Figure 11c), indicating stronger updrafts and more coherent plumes may be more effective at transporting slow momentum from the surface toward the mixed-layer top. This is in correspondence with the observational study by Lareau et al. (2018) who found that medium cloud cover cumulus (30%–50%) have largest skewness.

In the along-wind component of the momentum flux (Figure 11d), profiles are more similar, but there is less flux below $z/\eta = 0.7$ in the cumulus regimes (yellow/blue). Perhaps, because the wind profiles are already better mixed in these regimes (Figure 11a), there is less momentum flux generated within the mixed-layer.

The momentum tendency is determined by the negative flux divergence as:

$$\partial_t u_{\parallel}(z) \propto -\partial_z \overline{u'_{\parallel} w'}(z), \tag{3}$$

where $\partial_t = \frac{\partial}{\partial t}$, and similarly for ∂z. Faster decrease of the flux with height implies that $\partial_t u_{\parallel} < 0$: the wind speed in the direction of the mean flow reduces. The two convective cloud regimes thus experience a slightly greater friction throughout the mixed-layer.

7. Conclusion & Discussion

This study aims to answer: "Does the surface-layer wind shear and momentum flux profiles change in different cloud regimes?" In particular, we are motivated by the idea that convective clouds are associated with different momentum transport and winds in the layers below. To explore such statistical relationships, we used a long time record of observations and daily LES hindcasts, which allow us to group different cloud regimes together across a wide range of atmospheric states.

We designed an automated classification that flags a day as belonging to a convective cloud regime based on several criteria, including having a positive surface buoyancy flux during daytime, having a cloud base close to the theoretical LCL, and no cloud above 3 km. We contrasted these convective days—with two classes of cloud cover—to clear sky days and days not driven by convection that often have other types of clouds, such as mid or high-level cloud not rooted in the surface or mixed layer. In the LES, we removed all days where convection or the large scale forcing saturated the upper layer of the model domain, leading to less days falling into that category especially. It is these days with deeper and larger cloud regimes, for which the LES was not traditionally designed and for which the domain size is too limited.

Overall, we have confidence in the LES' skill to reproduce the type of clouds expected for certain weather regimes, and also the turbulence characteristics associated with clear-sky and shallow convective regimes. The wind, temperature, and humidity climatology and mean diurnal cycle of winds belonging to the different cloud regimes are very similar in LES and observations, even if the days within the classifications do not always match.

We find that clear sky days and shallow convective cloud days have a very similar diurnal cycle of the surface layer wind, with a large wind gradient during nighttime that is mixed away during daytime. Shallow cumulus days generally have weaker winds and larger buoyancy fluxes than clear-sky days, and therefore have a head start in mixing away the nighttime wind shear. They also produce a steady increase in mean surface layer winds during the afternoon associated with the development of a deeper boundary layer and presumably the entrainment of higher momentum air.

However, we must keep in mind that shallow cumulus days tend to be warmer days from late spring to early autumn. Hence, because of the larger insolation in these months, the average buoyancy flux is larger than that of the clear-sky regime that is better distributed over the year.

The factors that help form convective clouds in the first place such as large surface buoyancy fluxes also help reduce surface layer wind shear. By further grouping the data into different stability classes defined by the Obukhov length, we attempt to remove the influence of surface buoyancy fluxes and surface friction velocity (set by the large scale wind) on the wind gradients. Doing so shows that convective cloud regimes have smaller surface-layer wind gradients compared to clear sky days at a similar neutral or weakly unstable stability. We also find that the Monin Obukhov nondimensional wind gradient function ϕ_M, which relates the surface friction velocity to the surface layer wind gradient, is smaller for the convective cloud regimes. This would imply that for a similar wind gradient (large scale wind), more momentum flux is generated on those convective cloud days compared to clear sky days. It also suggests, as shown by Liu et al. (2019) and Fodor et al. (2019), that empirical Monin-Obukhov similarity functions do not explicitly include the effect of large scale up- and downdrafts associated with convective eddies (using the scaling of boundary layer depth) underestimate the momentum flux that is generated in the surface layer.

The nondimensional momentum flux profiles throughout the entire boundary layer in the direction of the mean near-surface wind are very similar for the different regimes at midday, which suggests that small-scale shear-driven momentum diffusion still dominates the momentum flux. Larger differences are found in the nondimensional crosswind momentum fluxes, where the clear-sky and shallow convective cloud regimes have much more momentum flux in the mixed layer. These regimes also have stronger updrafts. Compared to clear sky days and shallow cumulus days, the non-convective (cloud) regime has much more crosswind momentum transport extending beyond the mixed layer top: up to 30% of the surface momentum flux is still present in the cloud layer ($z\ /\ z_i\ = 1.3$).

A fair question to ask is whether the clouds themselves, by triggering larger or more effective momentum transport, lead to weaker surface wind shear, and thus whether these results could be generalized to other

locations over land. We cannot fully answer this question without a detailed budget study that samples the momentum tendencies introduced by convective and cloudy plumes and by small-scale turbulence in LES or by spectral analysis of the scales that contribute to the total momentum flux in observations and LES. However, we may point to a few recent studies that reveal the influence of convective momentum transport on near-surface winds.

A recent study using Atlantic-wide ICON-LES hindcasts reveals that dry convective plumes coupled to moist convection overhead carry significant fluxes that tend to accelerate near-surface winds (Helfer et al., 2021). A spectral decomposition of momentum fluxes by eddy sizes derived from LES of organized shallow convection in a cold air outbreak demonstrates that larger eddies are accompanied by a momentum flux profile that can maximize in the mixed layer and accelerate near-surface winds (Saggiorato et al., 2020).

Whether our results of Cabauw can be generalized depends on whether specific mechanisms are at play over the Netherlands, which drive both weaker surface layer wind shear and more shallow cumulus convection. A land-sea breeze effect could be at play, driving stronger onshore winds at daytime and moister airmasses that favor cumulus convection regardless of locally driven buoyancy fluxes. We suspect that mesoscales and regional scales can make a difference in the real world, but are not adequately captured in 10 min averages eddy-covariance flux data or small LES domains with cyclic boundary conditions (Dixit et al., 2021).

A number of efforts are underway that will address these challenges. Foremost, the Ruisdael Observatory (https://ruisdael-observatory.nl/) will realize near-real time DALES hindcasts with open boundaries at 100 m resolution over the entire Netherlands combined with a dense measurement network that includes scanning cloud radars and a wind lidar at Cabauw that are currently being analyzed.

Data Availability Statement

The observational data that support the findings of this study are openly available in KNMI Data Platform (KDP) at https://dataplatform.knmi.nl/dataset/?tags=insitu&tags=CESAR, with the exception of the LD40 ceilometer data and observed friction velocity data. These data can be found at https://doi.org/10.4121/14994534. The model is commercial property, and the data are therefore only available on request, which is handled via the data repository on https://doi.org/10.4121/14994588.v1.

Acknowledgments
This project has received funding from the European Research Council (ERC) under the European Union's Horizon 2020 research and innovation program (Starting Grant Agreement 714918). We want to thank three anonymous reviewers for their comments that improved this manuscript.

References

Arrillaga, J. A., de Arellano, J. V.-G., Bosveld, F., Baltink, H. K., Yagüe, C., Sastre, M., & Román-Cascón, C. (2018). Impacts of afternoon and evening sea-breeze fronts on local turbulence, and on co² and radon-222 transport. *Quarterly Journal of the Royal Meteorological Society*, *144*(713), 990–1011. https://doi.org/10.1002/qj.3252

Baas, P., Bosveld, F. C., Klein Baltink, H., & Holtslag, A. A. M. (2009). A climatology of nocturnal low-level jets at cabauw. *Journal of Applied Meteorology and Climatology*, *48*(8), 1627–1642. https://doi.org/10.1175/2009JAMC1965.1

Bolton, D. (1980). The computation of equivalent potential temperature. *Monthly Weather Review*, *108*(7), 1046–1053. https://doi.org/10.1175/1520-0493(1980)108<1046:tcoept>2.0.co;2

Bony, S., Stevens, B., Ament, F., Bigorre, S., Chazette, P., Crewell, S., et al. (2017). Eurec4a: A field campaign to elucidate the couplings between clouds, convection and circulation. *Surveys in Geophysics*, *38*(6), 1529–1568. https://doi.org/10.1007/s10712-017-9428-0

Bosveld, F. (1999). *The knmi garden experiment: Micro-meteorological observations 1988 - 1989 corrections* (Vol. WR 99-03; Tech. Rep.). KNMI. Retrieved from http://projects.knmi.nl/cabauw/insitu/observations/documentation/Cabauw_TR/Cabauw_TR.pdf

Bosveld, F. (2020). *The cabauw in-situ observational program 2000—Present: Instruments, calibrations and set-up* (Tech. Rep.). Retrieved from https://cdn.knmi.nl/knmi/pdf/bibliotheek/knmipubTR/TR384.pdf

Bosveld, F., Baas, P., Beljaars, A., Holtslag, A., Vila-Gerau de Arellano, J., & van de Wiel, B. (2020). Fifty years of atmospheric boundary-layer research at Cabauw Serving Weather, Air Quality and Climate. *Boundary-Layer Meteorology*, *177*, 583–612. https://doi.org/10.1007/s10546-020-00541-w

Bretherton, C., & Blossey, P. (2017). Understanding mesoscale aggregation of shallow cumulus convection using large-eddy simulation. *Journal of Advances in Modeling Earth Systems*, *9*(8), 2798–2821. https://doi.org/10.1002/2017ms000981

Brown, A. R. (1999). Large-eddy simulation and parametrization of the effects of shear on shallow cumulus convection. *Boundary-Layer Meteorology*, *91*(1), 65–80. https://doi.org/10.1023/a:1001836612775

Dixit, V., Nuijens, K. C., & Helfer, L. (2021). Counter-gradient momentum transport through subtropical shallow convection in icon-lem simulations. *Journal of Advances in Modeling Earth Systems*, *13*(6), e2020MS002352. https://doi.org/10.1029/2020MS002352

Fodor, K., Mellado, J. P., & Wilczek, M. (2019). On the role of large-scale updrafts and downdrafts in deviations from monin–obukhov similarity theory in free convection. *Boundary-Layer Meteorology*, *172*(3), 371–396. https://doi.org/10.1007/s10546-019-00454-3

He, Y., Monahan, H., & McFarlane, N. A. (2013). Diurnal variations of land surface wind speed probability distributions under clear-sky and low-cloud conditions. *Geophysical Research Letters*, *40*(12), 3308–3314. https://doi.org/10.1002/grl.50575

Helfer, K. C., Nuijens, L., & Dixit, V. (2021). The role of shallow convection in the momentum budget of the trades from large-eddy-simulation hindcasts. *Quarterly Journal of the Royal Meteorological Society*, *147*(737), 2490–2505. https://doi.org/10.1002/qj.4035

Heus, T., Van Heerwaarden, C., Jonker, H. J., Pier Siebesma, A., Axelsen, S., Dries, K., et al. (2010). Formulation of the Dutch atmospheric large-eddy simulation (dales) and overview of its applications. *Geoscientific Model Development*, *3*(2), 415–444. https://doi.org/10.5194/gmd-3-415-2010

Holloway, C. E., Wing, A. A., Bony, S., Muller, C., Masunaga, H., L'Ecuyer, T. S., et al. (2017). Observing convective aggregation. *Surveys in Geophysics*, *38*(6), 1199–1236. https://doi.org/10.1007/s10712-017-9419-1

Ifs documentation cy41r1. (2015). *Technical report*. Retrieved from https://www.ecmwf.int/node/9211, https://doi.org/10.21957/p50qmwprw

Jabouille, P., Redelsperger, J. L., & Lafore, J. P. (1996). Modification of surface fluxes by atmospheric convection in the TOGA COARE region. *Monthly Weather Review*, *124*(5), 816–837. https://doi.org/10.1175/1520-0493(1996)124<0816:mosfba>2.0.co;2

Lareau, N. P., Zhang, Y., & Klein, S. A. (2018). Observed boundary layer controls on shallow cumulus at the arm Southern Great Plains site. *Journal of the Atmospheric Sciences*, *75*(7), 2235–2255. https://doi.org/10.1175/jas-d-17-0244.1

LeMone, M. A. (1983). Momentum transport by a line of cumulonimbus. *Journal of the Atmospheric Sciences*, *40*(7), 1815–1834. https://doi.org/10.1175/1520-0469(1983)040<1815:mtbalo>2.0.co;2

LeMone, M. A., & Jorgensen, D. P. (1991). Precipitation and kinematic structure of an oceanic mesoscale convective system. Part i: Momentum transport and generation. *Monthly Weather Review*, *119*(11), 2638–2653. https://doi.org/10.1175/1520-0493(1991)119<2638:paksoa>2.0.co;2

LeMone, M. A., & Pennell, W. T. (1976). The relationship of trade wind cumulus distribution to subcloud layer fluxes and structure. *Monthly Weather Review*, *104*(5), 524–539. https://doi.org/10.1175/1520-0493(1976)104<0524:trotwc>2.0.co;2

Li, D., & Bou-Zeid, E. (2011). Coherent structures and the dissimilarity of turbulent transport of momentum and scalars in the unstable atmospheric surface layer. *Boundary-Layer Meteorology*, *140*(2), 243–262. https://doi.org/10.1007/s10546-011-9613-5

Liu, S., Zeng, X., Dai, Y., & Shao, Y. (2019). Further improvement of surface flux estimation in the unstable surface layer based on large-eddy simulation data. *Journal of Geophysical Research: Atmospheres*, *124*(17–18), 9839–9854. https://doi.org/10.1029/2018jd030222

Moeng, C.-H., & Sullivan, P. P. (1994). A comparison of shear-and buoyancy-driven planetary boundary layer flows. *Journal of the Atmospheric Sciences*, *51*(7), 999–1022. https://doi.org/10.1175/1520-0469(1994)051<0999:acosab>2.0.co;2

Romps, D. M. (2017). Exact expression for the lifting condensation level. *Journal of the Atmospheric Sciences*, *74*(12), 3891–3900. https://doi.org/10.1175/jas-d-17-0102.1

Rotunno, R., Klemp, J. B., & Weisman, M. L. (1988). A theory for strong, long-lived squall lines. *Journal of the Atmospheric Sciences*, *45*(3), 463–485. https://doi.org/10.1175/1520-0469(1988)045<0463:atfsll>2.0.co;2

Saggiorato, B., Nuijens, L., Siebesma, A. P., de Roode, S., Sandu, I., & Papritz, L. (2020). The influence of convective momentum transport and vertical wind shear on the evolution of a cold air outbreak. *Journal of Advances in Modeling Earth Systems*, *12*(6), e2019MS001991. https://doi.org/10.1029/2019ms001991

Schalkwijk, J., Bosveld, F., & Siebesma, P. (2010). Timescales and structures in vertical transport in the atmospheric boundary layer. *Citeseer*.

Schalkwijk, J., Jonker, H. J., Siebesma, A. P., & Bosveld, F. C. (2015). A year-long large-eddy simulation of the weather over Cabauw: An overview. *Monthly Weather Review*, *143*(3), 828–844. https://doi.org/10.1175/mwr-d-14-00293.1

Schemann, V., Ebell, K., Pospichal, B., Neggers, R., Moseley, C., & Stevens, B. (2020). Linking large-eddy simulations to local cloud observations. *Journal of Advances in Modeling Earth Systems*, *12*(12), e2020MS002209. https://doi.org/10.1029/2020MS002209

Schlemmer, L., Bechtold, P., Sandu, I., & Ahlgrimm, M. (2017). Uncertainties related to the representation of momentum transport in shallow convection. *Journal of Advances in Modeling Earth Systems*, *9*(2), 1269–1291. https://doi.org/10.1002/2017ms000915

Siebesma, A. P., Bretherton, C. S., Brown, A., Chlond, A., Cuxart, J., Duynkerke, P. G., et al. (2003). A large eddy simulation intercomparison study of shallow cumulus convection. *Journal of the Atmospheric Sciences*, *60*(10), 1201–1219. https://doi.org/10.1175/1520-0469(2003)60<1201:alesis>2.0.co;2

Stevens, B. (2007). On the growth of layers of non-precipitating cumulus convection. *Journal of the Atmospheric Sciences*, *64*(8), 2916–2931. https://doi.org/10.1175/jas3983.1

Stevens, B., Ackerman, A. S., Albrecht, B. A., Brown, A. R., Chlond, A., Cuxart, J., et al. (2001). Simulations of trade wind cumuli under a strong inversion. *Journal of the Atmospheric Sciences*, *58*(14), 1870–1891. https://doi.org/10.1175/1520-0469(2001)058<1870:sotwcu>2.0.co;2

Sullivan, P. P., McWilliams, J. C., & Moeng, C.-H. (1994). A subgrid-scale model for large-eddy simulation of planetary boundary-layer flows. *Boundary-Layer Meteorology*, *71*(3), 247–276. https://doi.org/10.1007/bf00713741

Tung, W.-W., & Yanai, M. (2002). Convective momentum transport observed during the toga coare iop. Part ii: Case studies. *Journal of the Atmospheric Sciences*, *59*(17), 2535–2549. https://doi.org/10.1175/1520-0469(2002)059<2535:cmtodt>2.0.co;2

van Stratum, B. J., de Arellano, J. V.-G., van Heerwaarden, C. C., & Ouwersloot, H. G. (2014). Subcloud-layer feedbacks driven by the mass flux of shallow cumulus convection over land. *Journal of the Atmospheric Sciences*, *71*(3), 881–895. https://doi.org/10.1175/jas-d-13-0192.1

Wu, X., & Yanai, M. (1994). Effects of vertical wind shear on the cumulus transport of momentum: Observations and parameterization. *Journal of the Atmospheric Sciences*, *51*(12), 1640–1660. https://doi.org/10.1175/1520-0469(1994)051<1640:eovwso>2.0.co;2

Zhang, Y., & Klein, S. A. (2013). Factors controlling the vertical extent of fair-weather shallow cumulus clouds over land: Investigation of diurnal-cycle observations collected at the arm Southern Great Plains site. *Journal of the Atmospheric Sciences*, *70*(4), 1297–1315. https://doi.org/10.1175/jas-d-12-0131.1

Zhu, P. (2015). On the mass-flux representation of vertical transport in moist convection. *Journal of the Atmospheric Sciences*, *72*(12), 4445–4468. https://doi.org/10.1175/jas-d-14-0332.1